BIOCHEMISTRY
including biophysical chemistry & molecular biology

Article

pubs.acs.org/biochemistry

Specificity and Promiscuity in Human Glutaminase Interacting Protein Recognition: Insight from the Binding of the Internal and C-Terminal Motif

Monimoy Banerjee,[†] David L. Zoetewey,[†] Mohiuddin Ovee,[†] Suman Mazumder,[†] Valery A. Petrenko,[‡] Tatiana I. Samoylova,[‡,§] and Smita Mohanty*[,†]

[†]Department of Chemistry and Biochemistry, Auburn University, Auburn, Alabama 36849, United States

[‡]Department of Pathobiology, College of Veterinary Medicine, Auburn University, Auburn, Alabama 36849, United States

[§]Scott-Richey Research Center, College of Veterinary Medicine, Auburn University, Auburn, Alabama 36849, United States

Supporting Information

ABSTRACT: A large number of cellular processes are mediated by protein−protein interactions, often specified by particular protein binding modules. PDZ domains make up an important class of protein−protein interaction modules that typically bind to the C-terminus of target proteins. These domains act as a scaffold where signaling molecules are linked to a multiprotein complex. Human glutaminase interacting protein (GIP), also known as tax interacting protein 1, is unique among PDZ domain-containing proteins because it is composed almost exclusively of a single PDZ domain rather than one of many domains as part of a larger protein. GIP plays pivotal roles in cellular signaling, protein scaffolding, and cancer pathways via its interaction with the C-terminus of a growing list of partner proteins. We have identified novel internal motifs that are recognized by GIP through combinatorial phage library screening. Leu and Asp residues in the consensus sequence were identified to be critical for binding to GIP through site-directed mutagenesis studies. Structure-based models of GIP bound to two different surrogate peptides determined from nuclear magnetic resonance constraints revealed that the binding pocket is flexible enough to accommodate either the smaller carboxylate (COO^-) group of a C-terminal recognition motif or the bulkier aspartate side chain (CH_2COO^-) of an internal motif. The noncanonical ILGF loop in GIP moves in for the C-terminal motif but moves out for the internal recognition motifs, allowing binding to different partner proteins. One of the peptides colocalizes with GIP within human glioma cells, indicating that GIP might be a potential target for anticancer therapeutics.

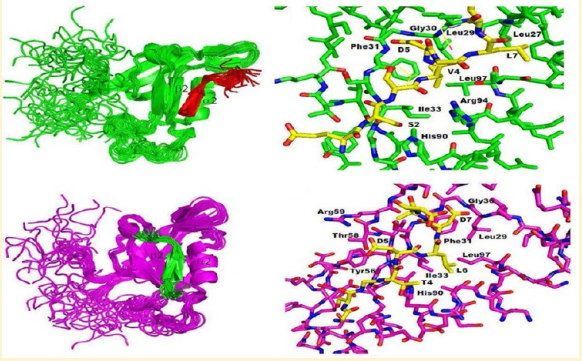

PDZ domains, which are named after founding members Post Synaptic Density 95, Discs Large, and Zonula Occludens-1, are one of the most important protein−protein interaction modules found in living systems. These domains act as a scaffold where signaling molecules are linked to a multiprotein complex. PDZ domains mediate this organization of signaling complexes by recognizing the C-terminal amino acid sequence motifs of the interacting protein.[1,2] The most important functions of PDZ domains appear to be localization and clustering of ion channels,[3] G-protein-coupled receptors,[4] and downstream effectors[5] at epithelial cell tight junctions, neuromuscular junctions, and postsynaptic densities of neurons.[6] These clustering and localization functions play significant roles in signal transduction pathways.[7]

Glutaminase interacting protein (GIP),[8] also known as tax interacting protein 1 (TIP-1),[9] is a small globular protein (124 amino acid residues) uniquely composed of one PDZ domain that is flanked by flexible N- and C-termini. PDZ domains are small (80−100 residues) protein−protein interaction modules that typically bind the C-terminal motifs of the interacting partner proteins[10] but on rare occasions may interact with internal motifs that mimic a C-terminus.[11,12] To date, GIP has been shown to interact only with the C-termini of a growing list of partner proteins, including glutaminase L,[8] HTLV-1 Tax,[9] HPV E6,[13] β-catenin,[14] Rhotekin,[15] FAS,[16] and KIR 2.3.[17] These GIP partner proteins play important roles in cell signaling, ion transport, transcription, and/or cancer. GIP has also been shown to act as a scaffold in both astrocytes and neurons.[18]

Discerning the protein interaction networks in and between different cell types forms the foundation for the design of new anticancer drugs. Thus, development of drugs targeting a specific protein can be achieved when its network is fully characterized to minimize unwanted side effects. To further explore the GIP interaction network, we used an f8-type phage display peptide library to screen for new GIP-binding peptides

Received: June 15, 2012
Revised: August 9, 2012
Published: August 10, 2012

   dx.doi.org/10.1021/bi3008033 | *Biochemistry* 2012, 51, 6950−6960

that may lead to new partner proteins. Such peptides may serve as leads for the development of novel anticancer therapeutics that specifically target GIP.

Here, we report the identification of 18 new GIP-binding peptides with novel internal motifs that map to a number of candidate human GIP partner proteins. All of these proteins are involved in various cancer pathways and/or other important cellular functions such as cellular adhesion, transcription, recombination, and cell death. Alanine replacement studies confirmed that the identified internal binding sequence motif is necessary for direct binding to GIP. Here, we report the structure-based models of the internal motif binding to a PDZ domain obtained from docking of the peptide to the protein using nuclear magnetic resonance (NMR) distance constraints obtained from intermolecular nuclear Overhauser effects (NOEs). Finally, we demonstrate that one of the peptides colocalizes with GIP inside human glioma cells and decreases their metabolic rate in culture.

EXPERIMENTAL PROCEDURES

Protein Expression and Purification. Expression and purification of GIP were conducted as described previously.[16] Briefly, the recombinant pET-3c/GIP plasmid was expressed in *Escherichia coli* BL21 DE3pLys cells, in M9 minimal medium containing ^{13}C-labeled glucose and/or ^{15}N-labeled ammonium chloride. The overexpressed recombinant GIP was purified in a single step by size exclusion chromatography on a Sephacryl S-100 column (GE Healthcare). Pooled fractions of the pure protein were exchanged with NMR buffer containing 50 mM sodium phosphate (pH 6.5), 1 mM EDTA, and 0.01% (w/v) NaN_3.

Screening of the Phage Display Peptide Library. For identification of GIP-binding peptides, a pVIII 9-mer phage display library was used.[19] The library contains 2×10^9 different phage clones with multivalently displayed foreign peptides, providing incredible diversity for finding target proteins under nonstringent conditions.[20] Prior to the library selection, GIP was purified as described above and dialyzed against 0.1 M phosphate buffer (pH 8.0). Two wells of a Medisorp 96-well plate were coated with the purified protein at a concentration of 100 μg/mL overnight at 4 °C. The protein-coated well was blocked with 1% bovine serum albumin (BSA) in Tris-buffered saline (TBS) for 1 h at room temperature. To select for the target-binding phage, an aliquot of 10^9 colony forming units (cfu) of the library (depleted on an unrelated target) was added to the well for an additional 1 h incubation at room temperature. After incubation, unbound phages were discarded and the wells were washed 10 times with TBS containing 0.1% Tween 20 (TBST). The bound phage was eluted with 0.2 M glycine (pH 2.2) for 10 min and immediately neutralized using 1 M Tris-HCl (pH 9.1). The eluted phages were amplified in *E. coli* K91BluKan bacteria, purified, and titered for the next round of selection. In rounds 2 and 3, 10^{10} cfu aliquots were used in the selection procedures. After round 3, phage DNA in the area of the *gpVIII* gene was amplified via polymerase chain reaction (PCR) from 33 random phage-infected bacterial colonies, purified, and sequenced. Sequences of GIP-binding peptides were deduced from phage DNA sequences using Chromas.

Phage Binding Assay. Medisorp 96-well plates were coated with GIP at a concentration of 70 μg/mL and 4 °C overnight and blocked with 1% BSA in TBS for 1 h at room temperature. An additional set of uncoated wells was also blocked for the negative control. The wells were washed twice with TBST washing buffer (pH 7.0). Each selected phage clone was amplified individually and added at a density of 5×10^6 cfu/well to the GIP-coated wells for 1 h incubation at room temperature. After incubation, the wells were washed 10 times with TBST washing buffer. Bound phage were recovered by adding 25 μL of lysis buffer [2.5% CHAPS and 0.1% BSA in TBS buffer (pH 7.0)] to the wells for 10 min at room temperature. After that, freshly prepared *E. coli* starved cells (125 μL/well) were added to the wells for 15 min to allow phage infection. Next, 180 μL of NZY broth (pH 7.5) containing 0.4 μg/mL tetracycline was added to each well, and the plates were placed in a 37 °C incubator for 45 min. Finally, the content of each well was plated on NZY plates containing 20 μg/mL tetracycline for overnight incubation at 37 °C. To quantify the phage, bacterial colonies were counted by a colony counter the next morning.

GIP−Peptide Titration by NMR. Interaction studies were conducted by titration of 100 μM GIP with peptides containing several different internal sequences: ESSVDLLDG, ASSSVDDMA, GTNLDGLDG, GSSLDVTDN, GSGTDLDAS, and GSSAAVTDN. The target peptides were obtained with >95% purity from Chi Scientific. The 10 mM stock solutions of these peptides were prepared in 10 mM phosphate buffer (pH 6.5). The amide chemical shift perturbations ($\Delta\delta$) were calculated as $\Delta\delta = |\Delta\delta^{15}\mathrm{N}|/f + |\Delta\delta^{1}\mathrm{H}|$.[16] The introduction of the f factor and its value were justified by the difference in the spectral widths of the backbone ^{15}N resonances and the ^{1}H signals (^{15}N range, 131.5 ppm − 100.8 ppm = 30.7 ppm; ^{1}H range, 10.1 ppm − 6.6 ppm = 3.5 ppm; correction factor f = 30.7/3.5 = 8.7). Thus, a correction factor f of 8.7 was used to give roughly equal weighting for each of the ^{1}H and ^{15}N chemical shift changes. For ligand titration experiments, uniformly ^{15}N-labeled GIP was titrated with increasing concentrations of peptide to a GIP:peptide ratio of 1:10, and the corresponding two-dimensional ^{1}H−^{15}N HSQC spectra were recorded. Beyond the ratio of 1:10, solid peptide was added in increasing amounts to an excess that approached saturation with protein:peptide ratios ranging from 1:40 to 1:140 for certain individual peptides.

GIP−Peptide Models. To model the structure of GIP in complex with ESSVDLLDG and GSGTDLDAS peptides, we performed the following experiments: two-dimensional (2D) TOCSY[21] and 2D ROESY[22] on each peptide, 2D ^{15}N/^{13}C F1, selectively-filtered NOESY,[23] three-dimensional (3D) ^{13}C-edited/filtered HSQC-NOESY, and 3D ^{15}N-edited/filtered HSQC-NOESY[24] on each peptide−protein complex. The sample contained ~400 μM uniformly ^{15}N- and ^{13}C-labeled GIP, unlabeled 8 mM ESSVDLLDG or 16 mM GSGTDLDAS, 50 mM phosphate buffer containing 5% D_2O (pH 6.5), 1 mM EDTA, and 0.01% (w/v) NaN_3. Peptide−peptide and peptide−protein NOEs were added to the set of previously determined protein NOEs from free GIP for structure calculation using ARIA.[25] Previous studies of the binding of GIP to various peptides by both X-ray crystallographic and NMR methods demonstrated that the core structure of GIP is not significantly affected by ligand binding.[26−28] In our previous study,[28] we determined the NMR structure of GIP in the free state and also in the bound state with a known ligand from the protein glutaminase using a whole new set of NOEs obtained from the NOESY data collected on the complex. The overall three-dimensional structures of GIP in both free and bound forms were the same except for minor conformational changes in the ligand binding regions of the protein in the bound form. The

dx.doi.org/10.1021/bi3008033 | *Biochemistry* 2012, 51, 6950−6960

NMR observation[28] was consistent with the results of X-ray structures of GIP bound with peptides from β-catenin[27] and KIR 2.3.[26] Thus, both NMR and X-ray studies showed that the overall structure of GIP remains unaffected except for minor conformational changes at the binding site to accommodate the ligand.[26−28] Additionally, the chemical shift perturbations of GIP titration with the three peptides mentioned above were reported to be significant only at or near the binding regions.[16,28] Interestingly, in this study, the chemical shift perturbations observed for GIP upon titration with the different internal motif peptides were very similar to what was observed previously for glutaminase, β-catenin, and KIR 2.3,[16,28] indicating that the overall structure of GIP remains unaffected except for the ligand binding regions. To build the NMR models of GIP complexed with two different ligands (two different internal motif peptides) accurately, we did not follow the usual procedure of simply docking the ligand to the 3D structure of a protein using the intermolecular NOE constraints between the protein and ligand. Instead, we removed the intra-NOE distance constraints of the regions of the protein (helix α2 and strand β2) that form the binding site. This approach provided flexibility to the regions of the protein involved in ligand binding, allowing them to adopt the conformational change induced upon ligand binding. Next, the experimentally derived intermolecular NOE constraints between GIP and each peptide (Table S1 of the Supporting Information) were added to the structure calculation process conducted with ARIA. We used 37 and 32 intermolecular NOE distance restraints that were experimentally identified between the ligand binding regions of the protein for each peptide in the two GIP−peptide complexes. The rest of the structure calculation process to determine the structure-based model of each complex was followed as described previously.[28] The experimental intermolecular NOE distance constraints described above were critical for the determination of the NMR models of the ligand-bound proteins that showed the ligand-induced conformational changes. The NMR experiments with free GIP and each GIP−peptide complex were conducted under identical conditions of pH, temperature, buffer, protein concentration, etc. On an iterative basis, the structures were evaluated and refinements made to the ARIA inputs using VMD[29] to visualize the structures. For the final ensemble of structures, of a total of 200 starting structures, 25 structures with the lowest energy were chosen for water refinement. Of those, 20 structures with the lowest energy were selected for analysis with Procheck.[30]

Fluorescence Spectroscopy. All fluorescence spectra were recorded on a PerkinElmer LS 55 luminescence spectrofluorometer at 25 °C. Titration experiments were conducted as described previously.[16] The dissociation constant K_D was determined using OriginPro version 6.1. The equation corresponding to a single binding site was used to fit the data as described previously.[31]

Immunocytochemical Localization of GIP in Cancer Cells. D54 MG human glioma cells were plated onto four-chamber slides (Nunc, Naperville, IL) at a density of 3×10^4 cells/chamber in Dulbecco's modified Eagle's medium (DMEM F-12) supplemented with 10% fetal bovine serum (FBS) and grown under 5% CO_2 at 37 °C for 24 h. For immunocytochemical localization of GIP, the cells were fixed with 1% paraformaldehyde in PBS for 30 min and then permeabilized with 0.5% Triton X-100 in PBS for 25 min at room temperature. The coverslips were blocked with MACS buffer [0.5% BSA and 2 mM EDTA in PBS (pH 7.2)] for 1 h. The cells were incubated with primary anti-GIP mouse monoclonal IgG (Novus Biologicals, Littleton, CO) diluted 1:15 in PBS with 1% BSA, overnight at 4 °C. The primary antibody was removed, and the slides were rinsed with PBS. Secondary goat anti-mouse Alexa 488-conjugated antibody (Novus Biologicals) diluted 1:40 in a PBS/BSA mixture was added and incubated for 1 h at room temperature. Unbound secondary antibody was removed by washing with PBS. Slides were mounted with coverslips using Vectashield DAPI mounting medium (Vector Laboratories, Inc., Burlingame, CA). Fluorescence images were acquired with an Olympus BH-2 fluorescence microscope equipped with a Nikon Digital Sight DS-L1 camera.

Peptide Internalization and Colocalization with GIP in Cancer Cells. To demonstrate the ability of the peptide to be internalized by human glioma D54 MG cells, the cells were plated on chamber slides and cultured overnight as described in the previous section. The cells were treated with the TAMRA-labeled ESSVDLLDGGG$(R)_7$ peptide at 1 μM for 25 min. After incubation, the cells were washed three times with PBS and fixed with 1% paraformaldehyde for 15 min. Fixed cells were mounted with coverslips using Vectashield DAPI mounting medium. The slides were evaluated by fluorescence microscopy.

For GIP−peptide colocalization studies, cells plated on chamber slides as described above were treated with the TAMRA-labeled ESSVDLLDGGG$(R)_7$ peptide at 1 μM for 25 min and fixed with 1% paraformaldehyde for 15 min, followed by three PBS rinses. Fixed cells were permeabilized with 0.5% Triton X-100 in PBS for 25 min, rinsed three times with PBS, and blocked with MACS buffer for 1 h at room temperature. The cells were then incubated with primary anti-GIP mouse monoclonal IgG antibody overnight at 4 °C and washed three times with PBS as described in the previous section. Fluorescein Alexa 488 anti-mouse secondary antibody was then added and incubated for 1 h at room temperature. After the cells had been washed three times with PBS, the cells were mounted and evaluated by fluorescence microscopy.

MTT Assay. The effect of the peptide on D54 MG cells was examined by an assay that utilizes MTT [3-(4,5-dimethylthiazol-2-yl)-2,5-diphenyltetrazolium bromide] (Sigma-Aldrich, St. Louis, MO) salt. This assay measures cellular oxidative metabolism. The dye is cleaved to a colored product by the activity of NAD(P)H-dependent dehydrogenase, and this indicates the level of energy metabolism in cells. The color development (yellow to blue) is proportional to the number of metabolically active cells. For these experiments, D54 MG cells were plated on 96-well culture plates at a density of 3×10^3 cells/well and cultured overnight in DMEM F-12 medium (Mediatech Inc., Manassas, VA) containing 10% fetal bovine serum at 37 °C. The next day, the peptide was added to the cells at concentrations of 10, 20, 40, 50, 75, 100, and 200 μM. The cells were incubated at 37 °C until the total treatment time reached 16 h. After that, a 10% volume of the MTT stock solution (5 mg/mL) was added to the cell cultures for 4 h for color development. The converted dye was then solubilized, and the absorbance was measured at 550 nm. Each data point was normalized against the control cells.

RESULTS

Identification of GIP-Binding Peptides by Phage Display. GIP-binding peptides were selected from an f8-type 9-mer phage display peptide library[32] that displays 4000 copies of the foreign nonamers in the N-terminal part of major coat

dx.doi.org/10.1021/bi3008033 | Biochemistry 2012, 51, 6950−6960

protein pVIII of phage fd-tet (landscape library). The library was constructed by replacement of amino acids 2−5 of pVIII with random nonamers. The landscape library allows selection of highly homologous families of peptides under nonstringent conditions because of its multivalency and avidity effect[20] with easily recognized binding motifs.[33] To reveal GIP-binding motifs, the gene *gpVIII* DNAs were amplified by PCR from 33 phage clones, sequenced, and translated into 18 unique peptide sequences. On the basis of sequence alignment, they were placed into two main groups (Table 1). Group 1 contained

Table 1. Peptide Sequences Identified for GIP Binding from a Phage Display Library Placed into Two Main Groups

Group 1	Group 2	Other
GGSSVDSEG	DSNLDVSVE	GSGTDLDAS
ESSVDLLDG	VSNLDTTND	
GSSSVDVDG	GTNLDGNGD	
AISSVDSMG	GSMNLDVQS	
ESSVDMIGD	GGNLDVNVG	
GSSVDLVGD	DGNLDSYDN	
AYESSVDDN		
ASSSVDDMA		
GSSLDVTSE		
GSSLDVTDN		
GYETSLDSN		

peptides with S/T-S-V/L-D (herein, three-letter codes are for the protein residues and single-letter codes are for the internal motif peptide residues) as a common motif. Interestingly, this motif was identified in different positions within the nine-amino acid peptide sequences, including 2−5, 3−6, and 4−7. Group 2 contained a three-residue N-L-D motif, which occupied positions 2−4 and 3−5 within the peptides. An additional sequence, GSGTDLDAS, was also identified. Comparative analysis of all sequences revealed S/T-X-V/L-D to be the consensus motif.

The specificity of the selected phage clones for GIP was confirmed through a phage binding assay by comparing the relative binding of individual phage clones to the target protein in comparison with the controls, BSA or empty wells of the plastic plates used for phage selection. As an additional control for binding specificity, this assay was repeated with phage f8-5, the vector that does not display any fusion foreign peptides.[19] Equal numbers of individual phage clones were added to the wells containing either GIP or the above controls followed by incubation and quantification of the bound phage by titering in the host *E. coli* K91BK cells. It was observed that GIP-selected clones do not bind either to BSA or to the plastic. The vector phage alone did not bind to GIP (data not shown).

Binding Affinities Determined by Fluorescence. Fluorescence assays involving titration of the protein to the peptides were conducted by monitoring the decrease in the protein fluorescence by the addition of increasing amounts of various peptides. The K_D values were calculated from the fluorescence intensity of GIP by plotting $(F_0 - F_C)/(F_0 - F_{min})$ versus [C], where F_0 and F_C are the fluorescence intensities of the free protein and the protein at a peptide concentration [C], respectively, and F_{min} is the fluorescence intensity upon saturation of all ligand binding sites of the protein.

A plot of $(F_0 - F_C)/(F_0 - F_{min})$ versus [C] was established using an equation that defines a single binding site. The data were fit to this plot to obtain the K_D values using OriginPro version 6.1. The K_D values of the internal motif peptides were within the range of 0.2−0.8 μM, suggesting a moderate affinity of GIP for these peptides.

GIP Binding to Internal Motif Peptides Monitored by NMR Spectroscopy. Several GIP-specific peptides revealed in the selection experiments were synthesized to assess their interactions with GIP using NMR spectroscopy. Five peptides representing motifs with either S/T or V/L amino acids at position P_{-2} or P_0 according to standard PDZ nomenclature[28] were selected for the NMR studies.

Chemical shift mapping is a powerful method frequently employed to investigate possible protein ligand interactions by NMR. The 2D $^1H-^{15}N$ HSQC spectrum provides the fingerprint region of a protein. This NMR experiment is a sensitive technique for studying protein−ligand interactions in solution.[16,28,34] Any perturbation in the chemical shift resonances from their original positions in this region indicates a change in the local environment of the affected residues within a protein.[16] On the basis of the local chemical shift changes, we know that the overall fold and shape of the protein

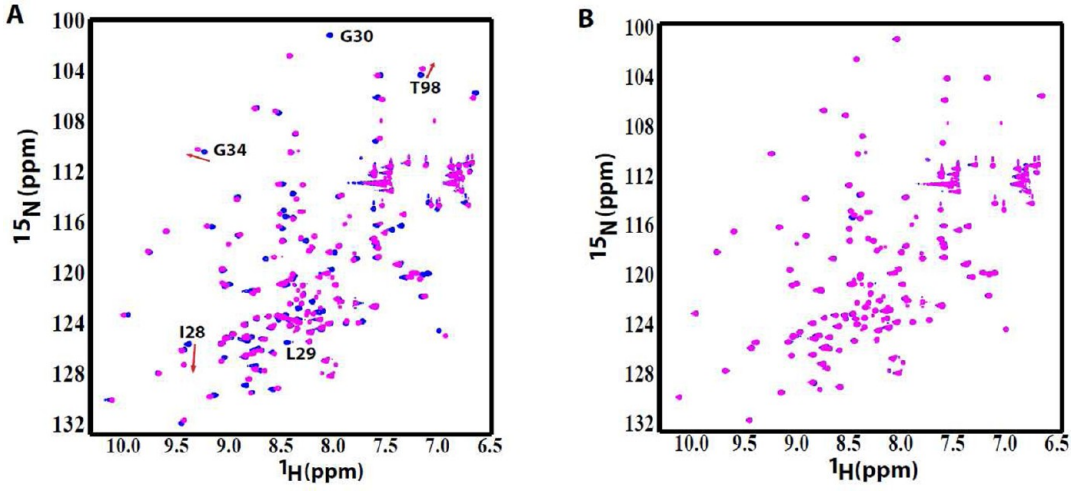

Figure 1. GIP PDZ domain shows a direct interaction with the GSSLDVTDN internal motif peptide but not with the doubly substituted GSSAAVTDN peptide. (A) ^{15}N HSQC spectra of the ^{15}N-labeled GIP PDZ domain alone (blue) and with the GSSLDVTDN peptide (magenta). (B) ^{15}N HSQC spectra of the ^{15}N-labeled GIP PDZ domain alone (blue) and with the GSSAAVTDN peptide (magenta).

dx.doi.org/10.1021/bi3008033 | *Biochemistry* 2012, 51, 6950−6960

Table 2. Chemical Shift Perturbations of GIP Residues upon Binding to Internal Motif Peptides

peptide	medium shifted (>0.1 ppm) residues/regions	large shifted (>0.2 ppm) residues/regions	residues in intermediate exchange
ASSSVDDMA	Ile18, His19, Lys20, Arg22, Gln23, Gly34, Ile55, Val57, Leu71, Thr86, Val88, Arg96, Thr98, Ser101, Glu102	Asn26, Leu27, Ile28, Phe31, Ser32, Ile33, Gly35, Thr58, Glu67, Arg94, Leu97, Arg100	Leu29, Gly30
ESSVDLLDG	Ile18, His19, Lys20, Arg22, Gly34, Gly36, Phe46, Tyr56, Val57, Thr58, Val60, Glu62, Glu67, Leu71, Thr86, Arg96, Leu97, Thr98, Lys99, Ser101	Asn26, Leu27, Arg94, Arg100	Ile28, Leu29, Gly30, Phe31, Ser32, Ile33
GSGTDLDAS	Glu17, Ile28, Gly34, Gly36, Ile55, Val57, Thr58, Ser61, Glu62, Leu71, Ile77, Thr86, Thr98	Phe31, Ser32, Ile33, Glu67, Arg94, Arg96	Leu29, Gly30
GTNLDGNGD	Glu17, Phe31, Gly34, Gly36, Ile55, Val57, Thr58, His90, Arg96, Thr98	Ser32, Ile33, Glu67, Arg94	Leu29, Gly30
GSSLDVTDN	Phe31, Ile33, Gly36, Thr58, Ser61, Glu67, His90, Arg94, Arg96, Thr98, Lys99	Leu27, Ile28, Ser32	Leu29, Gly30

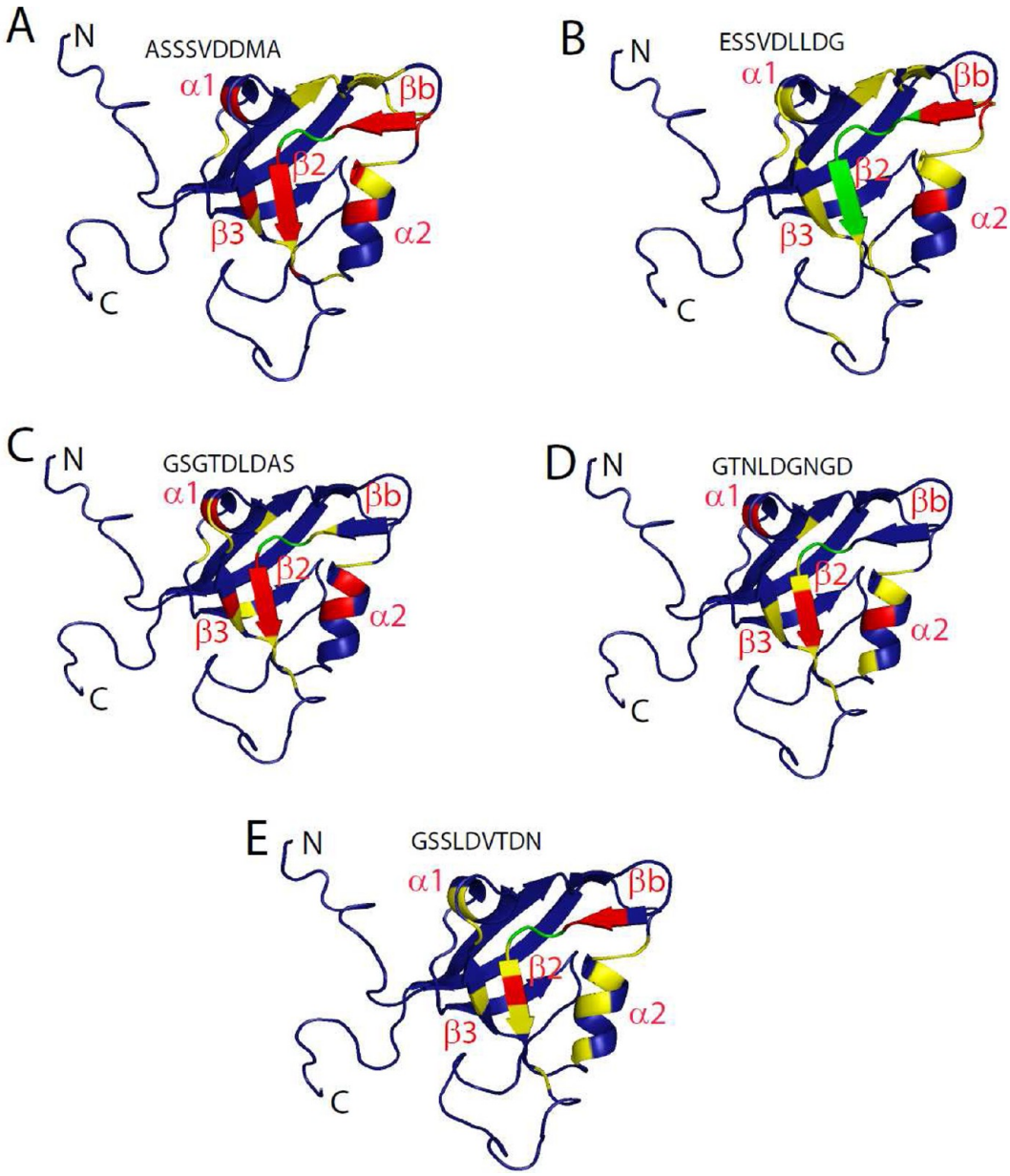

Figure 2. Magnitudes of the amide chemical shift changes represented in different colors on a ribbon diagram of GIP bound to the various internal motif peptides: (A) ASSSVDDMA, (B) ESSVDLLDG, (C) GSGTDLDAS, (D) GTNLDGNGD, and (E) GSSLDVTDN. Red indicates a $\Delta\delta$ of >0.2 ppm, yellow a $\Delta\delta$ between 0.1 and 0.2 ppm, blue a $\Delta\delta$ of <0.1 ppm, and green intermediate exchange. Selected secondary structural elements are labeled in red.

dx.doi.org/10.1021/bi3008033 | *Biochemistry* 2012, 51, 6950−6960

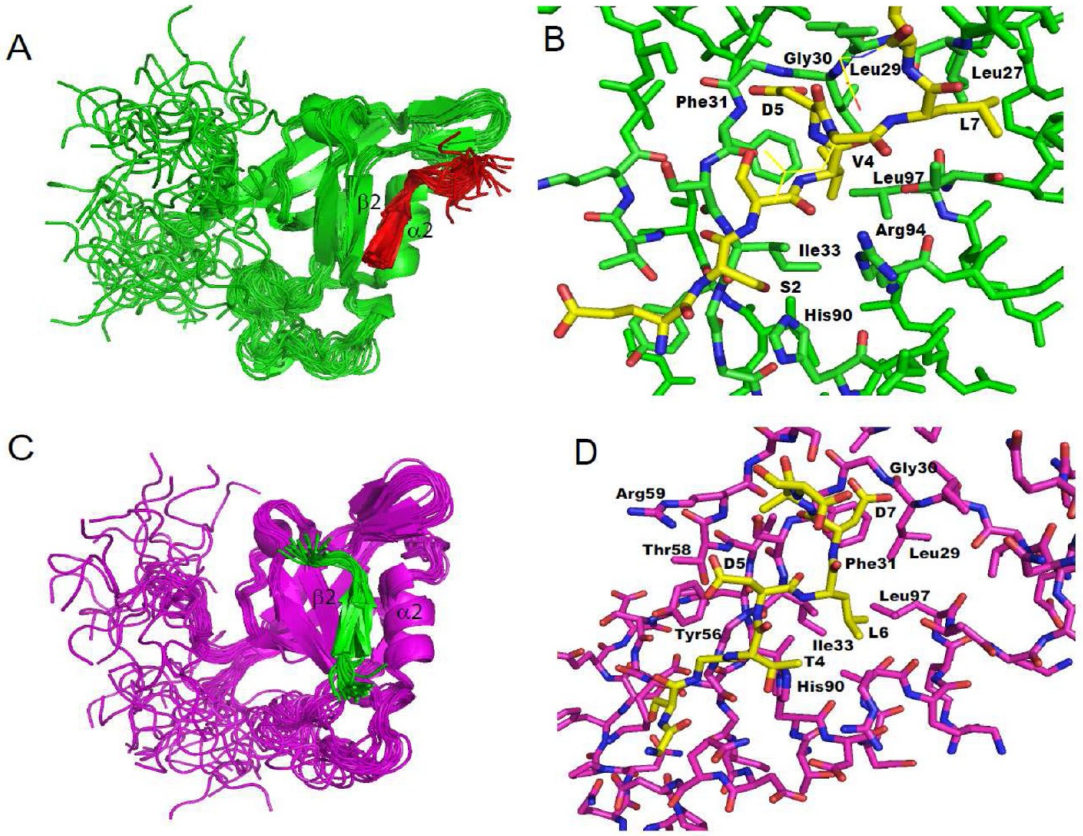

Figure 3. Structures of GIP−ESSVDLLDG and GIP−GSGTDLDAS complexes. (A) Ensemble of the 20 lowest-energy structures of the GIP−ESSVDLLDG complex. (B) D at position P_1 forms hydrogen bonds with Leu29 and Gly30 HN and S at position P_2 with His90. V at position P_0 buries itself into a hydrophobic pocket created by Leu29, Phe31, Ile33, and Leu97. (C) Ensemble of the 20 lowest-energy structures of the GIP−GSGTDLDAS complex. (D) D at position P_1 forms hydrogen bonds with Leu29 and Gly30 HN and T at position P_2 with His90. L at position P_0 buries itself into a hydrophobic pocket created by Leu29, Phe31, Ile33, and Leu97.

remain unchanged upon ligand binding as similar chemical shift changes were observed for GIP−peptide complexes with C-terminal peptides from glutaminase L,[28] KIR 2.3,[16] and *β*-catenin.[16] The chemical shift perturbation results suggesting structural changes only at or near the binding site within the protein when bound to any of the above mentioned three peptides are consistent with the structural studies conducted by NMR[28] and X-ray studies.[26,27] To elucidate a molecular mechanism of GIP−ligand binding, we studied the interaction of GIP with selected peptides by 2D HSQC titration experiments. The amide proton and nitrogen resonances in the HSQC spectra were followed for each titration point. Resonances from most of the residues of GIP followed fast exchange kinetics on the NMR time scale as observed by gradual and systematic changes in their chemical shift positions (Figure 1A). A few specific residues such as Leu29 and Gly30 followed intermediate exchange kinetics as seen by the disappearance of these peaks (Figure 1A). The decrease in peak intensity of these residues is due to the exchange between amide resonances of free and bound GIP. Residues Leu29 and Gly30 are a part of the ILGF binding loop that makes specific hydrogen bonds to the negatively charged terminal carboxylate group of the partner protein with a C-terminal recognition motif during binding.[28] This causes large chemical shift perturbations in these residues[35] despite very small structural changes.[26−28] For our titration experiments, the magnitude of changes in the chemical shifts of residues in GIP can be correlated to the relative proximity to the peptide in the complex.

Chemical Shift Perturbation of GIP upon Binding to Internal Motif Peptide Ligands. The chemical shift perturbation for each residue was calculated from the chemical shift changes of both ^{1}H and ^{15}N nuclei. When internal motif peptides were added, systematic changes in the amide resonances occurred in the titration spectra (Figure S1 of the Supporting Information). The significant chemical shift perturbations were grouped into three categories: medium shifted (>0.1 ppm), large shifted (>0.2 ppm), and intermediate exchange (Table 2). The intermediate exchange for certain residues within or very near the ILGF loop indicates that this loop is highly flexible as it has kinetic properties dramatically different from those of the rest of the protein. Unfortunately, because of the intermediate exchange that greatly broadens the resonances, the exact kinetic parameters of this region could not be studied. The magnitudes of the amide chemical shift changes upon binding to different internal motif peptides are mapped onto the ribbon diagram of GIP as indicated by different colors (Figure 2).

Chemical shift perturbation analysis shows that the ILGF loop, *β*2 strand, and *α*2 helix are the regions of GIP that are most affected. It also shows that residues Ile18−Gln23, Ile55−Glu62, and Glu67, which belong to the *β*1, *β*a, and *β*3 strands as well as the *α*1 helix, are also affected, but to a lesser extent. This observation suggests that the peptides with internal

dx.doi.org/10.1021/bi3008033 | *Biochemistry* 2012, 51, 6950−6960

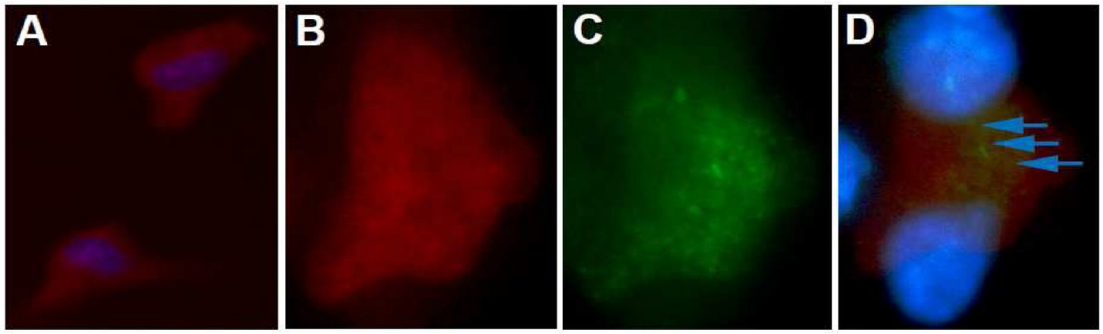

Figure 4. Localization of GIP and a GIP-binding peptide ESSVDLLDG in D54 MG human glioma cells. (A) Internalization of the peptide by glioma cells. The peptide was labeled with TAMRA and is shown inside the cells as red fluorescence. (B) The ESSVDLLDG peptide was localized in the cytoplasm of the glioma cell (red). (C) GIP was localized in the cytoplasm of the same cell using primary anti-GIP antibody followed by secondary antibody conjugated to Alexa 488 (green). (D) Merged image of panels B and C showing colocalization (indicated with arrows) of GIP and the ESSVDLLDG peptide within the cell. Cell nuclei were stained with DAPI (blue).

binding motifs bind to the same binding site nestled between the β2 strand and α2 helix of GIP as the canonical C-terminal motif. This binding is allosterically driven, reminiscent of the way GIP binds to C-terminal motifs.[16,26−28]

Role of the Residues at Positions P_0 and P_1 of the Peptide in GIP−Peptide Binding. To analyze the role of specific residues in the internal motif recognition by GIP, we created a double alanine substitution for LD in the GSS**LD**VTDN peptide. NMR titrations were performed to determine the effect of these substitutions on GIP binding. GIP was titrated with various concentrations of the alanine-substituted peptide GSS**AA**VTDN. Compared to that of the wild-type GSSLDVTDN peptide (Figure 1A), the chemical shift perturbation is negligible for the AA substitution (Figure 1B). This indicates that any interaction between the peptide and GIP was completely eliminated. Interestingly, the observation that the GSS**AA**VTDN peptide has virtually no binding to GIP suggests that both L and D are important for optimal interactions. Titrations with each of the identified peptides show that Leu29 and Gly30 are always in intermediate exchange (Table 2). Because LD or VD is present in each peptide and Leu29 and Gly30 are in intermediate exchange for the titration of each peptide, this supports our hypothesis that LD interacts directly with Leu29 and Gly30 of the ILGF carboxylate binding loop as a mimic of a hydrophobic C-terminal residue from a canonical C-terminal motif.

Structural Characterization of Internal Motif Recognition by GIP. Structure-based models of GIP bound to each of the two internal motif peptides were obtained through docking studies using intermolecular NOEs measured by NMR. These docking studies used experimentally derived NOE distance restraints that provided the details of the interactions between each internal motif peptide and the GIP protein. We also used the intrapeptide NOEs from the peptide while it was bound to GIP to determine the internal structure of each peptide in the complex. The chemical shift perturbations of GIP binding to the internal motif peptides ESSVDLLDG and GSGTDLDAS were separately mapped onto the same region as that of the C-terminal peptides reported earlier by our laboratory.[16,28] The chemical shift perturbation studies detailing the regions of the GIP protein that were most affected upon binding to the internal motif peptides showed patterns similar to those for previously determined complexes of GIP with C-terminal binding peptides.[16,28] This similarity in binding patterns allowed us to use our previously determined structure of the protein as a starting point in our structure-based model using the experimentally derived intermolecular NOEs between the GIP protein and each of the internal motif peptides. The experimentally derived NOEs demonstrated that each peptide bound to the protein in an extended strand conformation analogous to the previously determined C-terminal binding peptides (Table S1 of the Supporting Information). There are four critical points of contact between GIP and both internal motif peptides. First, the peptide binds by β-strand addition to form an antiparallel β-sheet with the β2 strand from GIP. Both peptides bind to GIP as antiparallel β-strands through this process. Second, the hydrophobic residue at position P_0 buries itself into the hydrophobic pocket created by Leu29, Phe31, Leu97, and Ile33. For ESSVDLLDG and GSGTDLDAS, the role of position P_0 is taken by V4 and L6, respectively. Both side chains bury themselves into the hydrophobic pocket in the same way and with the same relative orientation. Third, either S or T at position P_{-2} forms a hydrogen bond with His90 at the α2:1 position in GIP. Both ESSVDLLDG (Figure 3A,B) and GSGTDLDAS (Figure 3C,D) have more than one S or T in their respective sequences, but it is S2 and T4 that are at position P_{-2} from V4 and L6 at position P_0 within each peptide. The fourth and perhaps most important key point of contact is between the negatively charged carboxylate group of the ligand and the backbone amides from Leu29 and Gly30 within the ILGF loop of GIP. For canonical binding, this takes place with the C-terminal carboxylate of the interacting partner.[28] For the internal recognition motifs, the side chain of aspartate acts as a substitute for the C-terminus. This role is played by D5 and D7 in ESSVDLLDG and GSGTDLDAS, respectively. To bind to the side chain carboxylate in an internal recognition motif, the flexible loop between the noncanonical βb and β2, which includes residues Leu29 and Gly30 in the ILGF loop, adjusts slightly so that the amide protons orient themselves toward the side chain carboxylate to form a set of hydrogen bonds similar to the set of hydrogen bonds formed to the C-terminus during canonical binding.

Colocalization of GIP and the Internal Motif Peptide in Human Glioma Cells. GIP has been reported to be involved in many cancer pathways and represents a promising drug target.[14,36,37] Our searches of protein databases (UniProt) indicated multiple cancer-related proteins containing the novel internal motif identified through our phage library screen (Table S2 of the Supporting Information). We studied the intracellular distribution of one of the peptides in human D54

MG glioma cells. The cells were treated with a synthetic ESSVDLLDG peptide fused to a cell-penetrating peptide G_2R_7 labeled with TAMRA. By fluorescence microscopy, the labeled peptide was shown to be uniformly distributed in the cytoplasm of the glioma cells (Figure 4A). Next, cultures of D54 MG cells were treated with the TAMRA-labeled peptide followed by GIP staining with an anti-GIP antibody detected with a secondary antibody conjugated to Alexa 488 (Figure 4). Both, the peptide (red) and GIP (green), were found to be colocalized in the cytoplasm of the cells. To investigate whether the peptide mentioned above will have any effect on the glioma cells, the cells were treated with the peptide at concentrations ranging from 10 to 200 μM for 16 h and their metabolism was measured by the MTT assay. The cell metabolism was suppressed in a dose-dependent manner with increasing peptide concentrations (Figure 5). The peptide concentration required to suppress 50% of the cell metabolism (IC_{50}) was found to be equal to 69 ± 10 μM.

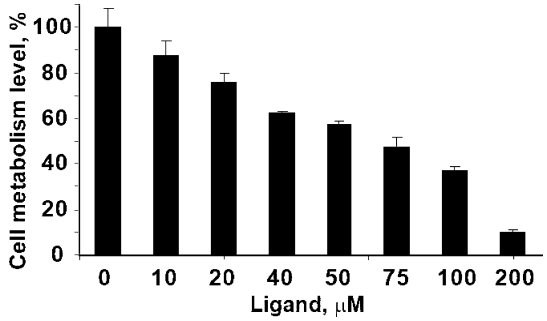

Figure 5. Effect of the ESSVDLLD peptide on the cellular metabolism of D54 MG human glioma cells. The peptide was added to the cells at different concentrations ranging from 10 to 200 μM. Cell metabolism was assessed using the MTT assay and expressed as a percentage of the mean absorbance measured in untreated control cell cultures.

DISCUSSION

Internal Motif Recognition by GIP. In this study, an f8/9 phage landscape library with multivalently displayed foreign nonamers was used to identify new binding motifs for GIP, a single-PDZ domain-containing protein. The library used here was diverse, composed of 2 billion different phage clones. A randomized DNA segment was inserted into the N-terminus of the *gpVIII* gene that encodes the major phage coat protein.[32] PDZ-binding phage clones were isolated from the library in three successive rounds of biopanning. In the GIP−phage binding assay, all of the selected phage clones were confirmed to be specific for GIP. Analysis of the peptide sequences led to the identification of a consensus internal-binding motif S/T-X-L/V-D. In the majority of previously reported phage display studies of PDZ-binding motifs, the identified peptide ligands were C-terminal recognition motifs.[6,38] To the best of our knowledge, this is the first report of GIP recognition of internal binding motifs. In the selected sequences, S or T, which were followed by variable amino acids at position P_{-1}, always occupied position P_{-2}. Position P_0 was always occupied by V or L, but not by I. This might indicate that steric factors are involved in binding; thus, only the symmetric V or L side chains fit into the hydrophobic cavity, but not the asymmetric I side chain. Aspartate at position P_1 was absolutely required.

Mechanisms of Internal Motif Recognition and Comparison with Canonical C-Terminal Recognition by GIP. Here, we also report structure-based models of PDZ domain recognition by two distinct internal motif peptides (Figure 3). The binding of ESSVDLLDG and GSGTDLDAS to GIP shows key similarities to and differences from the canonical PDZ C-terminal binding by GIP with its interacting partner proteins. The similarities include the β-strand addition mechanism, S or T at position P_{-2} forming a hydrogen bond with His90, and V or L at position P_0 binding within the hydrophobic pocket created by Leu29, Phe31, Ile33, and Leu97. This explains the similar pattern of chemical shift perturbations within GIP for the binding of different internal motif peptides. The key difference is that in an internal motif P_0 is not the C-terminus with a free carboxylate group. Instead, a hydrophobic residue at position P_0 and D at position P_1 serve as a structural mimic of a C-terminus with the side chain carboxylate group of D forming the same set of hydrogen bonds to the backbone amides from Leu29 and Gly30 within the ILGF binding loop. Aspartate at position P_1 has a different geometry than a C-terminal carboxylate group and needs to accommodate four additional heavy atoms. As a result, the backbone atoms of V or L at position P_0 and D at position P_1 of the peptide loop around so that the side chain carboxylate group of D at position P_1 points back toward the binding pocket. Analysis of the identified phage sequences shows that D is absolutely conserved among all the internal binding motifs. Each synthetic peptide derived from a phage clone did bind to GIP as monitored by NMR titrations. Thus, while E is also negatively charged, it appears that its side chain is simply too bulky for the geometry to be accommodated in the binding pocket in an energetically favorable way.

Furthermore, while both Leu29 and Gly30 make the same set of hydrogen bonds to either a canonical C-terminal carboxylate group or a carboxylate group from the side chain of D at position P_1 for an internal motif, the ILGF loop appears to be somewhat flexible and accommodating. It moves in to bind to a terminal carboxylate group of a C-terminal motif or moves out to bind to a carboxylate group from D at position P_1 of an internal motif. The flexibility of this loop may be due to the noncanonical βa−βb hairpin loop of GIP. In most PDZ domains, the GLGF motif, also known as the carboxylate-binding loop, comes directly between β1 and β2. However, in GIP, the noncanonical βa−βb hairpin loop uniquely positions the ILGF carboxylate-binding loop at a pivot point between βb and β2, thus allowing it to accommodate both sets of geometries either a terminal carboxylate group of the C-terminal motif or a side chain carboxylate group of D at position P_1 for an internal motif.

Previously, X-ray crystal structures of a PDZ domain with internal motifs were determined.[11,12,39] X-ray structures show that GLGF motif plays an important role for the interaction process. Interestingly, our GIP−peptide model suggests that the ILGF motif of GIP moves out to accommodate the internal motif. This flexible nature of the GLGF/ILGF motif helps to recognize both C-terminal and internal motif ligands.

Comparison of the Binding of the ESSVDLLDG and GSGTDLDAS Peptides to GIP. Both ESSVDLLDG and GSGTDLDAS bind as part of an antiparallel β-sheet to the β2 strand. However, after position P_1, the C-terminal segments of the peptides diverge in different directions. The direction of divergence appears to be controlled by whether L or V occupies at position P_0. For ESSVDLLDG, the alignment of V at

position P_0 in the hydrophobic pocket of GIP followed by the alignment of D at position P_1 allows the rest of the peptide to continue roughly antiparallel to βb. The hydrophobic L at position P_3 makes a hydrophobic contact with Leu27 that further contributes to the binding stability of this particular peptide with GIP. In the case of GSGTDLDAS, the positioning of the larger hydrophobic residue L at position P_0 into the hydrophobic pocket causes D at position P_1 to be positioned such that the remaining A and S at positions P_2 and P_3 point away orthogonal to both βb and β2. Also in contrast to ESSVDLLDG, GSGTDLDAS appears to form a slightly more extended antiparallel β-sheet with β2. Overall, it appears that for binding to GIP the following conditions must be met: the ability to form a β-strand and the sequence S/T-X-L/V-D. ESSVDLLDG has both VD and LD pairs in its sequence, but only VD binds to the ILGF loop because it contains S at relative position P_{-2}. However, if the LD pair was bound to the ILGF loop, D would be at position P_{-2} instead of S, which is not energetically favorable because His90 is present at position α2:1. The His90 at position α2:1 is responsible for the selectivity of S/T at position P_{-2} of the interacting partner.

Evidence of Internal Motif Recognition by GIP. Very interestingly, endonuclein, a cell cycle-regulated WD-repeat protein, was recently reported to interact with GIP.[40] Endonuclein does not contain a canonical C-terminal PDZ binding motif but contains the sequence EISGLDL (residues 387−393) within its five WD repeats. WD repeats are β-sheet domains that contain multiple β-hairpin turns. It is possible that endonuclein interacts with GIP through this region that serves as an internal motif. If confirmed, this would be the first independent example of an interaction of GIP with a noncanonical internal motif.

Colocalization of GIP and the Internal Motif Peptide. GIP was shown to have the same subcellular localization (Figure 4) as the synthetic peptide, ESSVDLLDG. The peptide was found to inhibit the metabolism of the glioma cells in a preliminary test.

New Potential Partner Proteins of GIP. Using protein database searches, we have identified several proteins with the S/T-X-V/L-D internal motif that were previously shown to be involved in various cancer pathways and tumorigenesis (Table S2 of the Supporting Information). For example, a reduced level of expression of the mediator complex subunit 1 (MED 1) protein containing the motif described above was associated with a more pronounced tumorigenic phenotype in human melanoma cells.[41] The CYLD gene that encodes the cylindromatosis 1 protein also has this motif and was found to be downregulated in human hepatocellular carcinoma cells and involved in their apoptotic resistance.[42] A growing body of evidence indicates that CYLD deficiency may promote the development of various cancers.[43] Another S/T-X-V/L-D internal motif-containing protein, MYO18B, was suggested to act as a tumor suppressor in the development of lung cancer.[44] The MYO18B protein was also shown to play an essential role in ovarian cancer.[45]

CONCLUSIONS

Our studies reveal a new internal recognition motif for GIP. GIP recognizes target proteins containing the S/T-X-V/L-D internal motif. This is the first report of GIP recognition of an internal motif. We have identified 18 new target proteins containing this internal motif expanding the GIP interaction network. Structure-based models of GIP−peptide complexes reveal that the binding pocket of GIP is flexible and can accommodate either C-terminal or internal recognition motifs. The involvement of GIP in many cancer pathways suggests that this protein might be a potential target for drug design.

ASSOCIATED CONTENT

Supporting Information

Chemical shift perturbation profiles of GIP upon binding to various internal motif peptides, tables of NMR and refinement statistics for GIP with the internal motif peptides ESSVDLLDG and GSGTDLDAS, and tables of human proteins that have homologies with GIP-binding peptides identified via phage display. This material is available free of charge via the Internet at http://pubs.acs.org.

AUTHOR INFORMATION

Corresponding Author

*Department of Chemistry and Biochemistry, Auburn University, Auburn, AL 36849. Phone: (334) 826-7980. E-mail: mohansm@auburn.edu.

Author Contributions

S. Mohanty conceived and designed the research plan. T.I.S. designed the phage display part of the study, and V.A.P. provided the phage display peptide library and protocols. M.B. and S. Mazumder prepared GIP proteins in the Mohanty laboratory. M.B. performed phage display experiments and cell-based assays in the Samoylova laboratory. M.B. and D.L.Z. performed NMR experiments, data processing, and analysis in the Mohanty laboratory. M.B. analyzed NMR titration data in the Mohanty laboratory. D.L.Z. analyzed and assigned NMR data and determined 3D models of the complex in the Mohanty laboratory. M.O. worked with ARIA in the Mohanty laboratory. T.I.S. and M.B. performed analysis of phage display data. M.B., D.L.Z., M.O., V.A.P., T.I.S., and S. Mohanty wrote the paper. M.B. and D.L.Z. made equal contributions to this work.

Funding

This research was financially supported by U.S. Department of Agriculture (USDA) PECASE (Presidential Early Career Award for Scientists and Engineers) Award 2003-35302-12930, National Science Foundation Grant IOS-0628064, USDA Grant 2011-65503-20030, and National Institutes of Health Grant DK082397 to S. Mohanty.

Notes

The authors declare no competing financial interest.

ACKNOWLEDGMENTS

We thank Dr. Alexandre Samoylov, Ms. Nancy Morrison, and Ms. Anne Cochran for their consultations and technical help. We thank Dr. Uma V. Katre for critical reading of the manuscript.

ABBREVIATIONS

PDZ, Post Synaptic Density 95, Discs Large, Zonula Occludens-1; GIP, glutaminase interacting protein; TIP-1, tax interacting protein-1; BSA, bovine serum albumin; TBS, Tris-buffered saline; TBST, TBS with 0.1% Tween 20; cfu, colony forming unit; DMEM, Dulbecco's modified Eagle's medium; FBS, fetal bovine serum; TAMRA, carboxytetramethylrhodamine; MTT, 3-(4,5-dimethylthiazol-2-yl)-2,5-diphenyltetrazolium bromide.

REFERENCES

(1) Kim, E., Niethammer, M., Rothschild, A., Jan, Y. N., and Sheng, M. (1995) Clustering of Shaker-type K^+ channels by interaction with a family of membrane-associated guanylate kinases. *Nature 378*, 85−88.

(2) Kornau, H. C., Schenker, L. T., Kennedy, M. B., and Seeburg, P. H. (1995) Domain interaction between NMDA receptor subunits and the postsynaptic density protein PSD-95. *Science 269*, 1737−1740.

(3) Le Maout, S., Welling, P. A., Brejon, M., Olsen, O., and Merot, J. (2001) Basolateral membrane expression of a K^+ channel, Kir 2.3, is directed by a cytoplasmic COOH-terminal domain. *Proc. Natl. Acad. Sci. U.S.A. 98*, 10475−10480.

(4) Zhong, H., and Neubig, R. R. (2001) Regulator of G protein signaling proteins: Novel multifunctional drug targets. *J. Pharmacol. Exp. Ther. 297*, 837−845.

(5) Wu, M., and Herman, M. A. (2007) Asymmetric localizations of LIN-17/Fz and MIG-5/Dsh are involved in the asymmetric B cell division in *C. elegans*. *Dev. Biol. 303*, 650−662.

(6) Fuh, G., Pisabarro, M. T., Li, Y., Quan, C., Lasky, L. A., and Sidhu, S. S. (2000) Analysis of PDZ domain-ligand interactions using carboxyl-terminal phage display. *J. Biol. Chem. 275*, 21486−21491.

(7) Kim, E., and Sheng, M. (2004) PDZ domain proteins of synapses. *Nat. Rev. Neurosci. 5*, 771−781.

(8) Olalla, L., Aledo, J. C., Bannenberg, G., and Marquez, J. (2001) The C-terminus of human glutaminase L mediates association with PDZ domain-containing proteins. *FEBS Lett. 488*, 116−122.

(9) Rousset, R., Fabre, S., Desbois, C., Bantignies, F., and Jalinot, P. (1998) The C-terminus of the HTLV-1 Tax oncoprotein mediates interaction with the PDZ domain of cellular proteins. *Oncogene 16*, 643−654.

(10) Lee, H. J., and Zheng, J. J. (2010) PDZ domains and their binding partners: Structure, specificity, and modification. *Cell Commun. Signaling 8*, 8.

(11) Zhang, Y., Appleton, B. A., Wiesmann, C., Lau, T., Costa, M., Hannoush, R. N., and Sidhu, S. S. (2009) Inhibition of Wnt signaling by Dishevelled PDZ peptides. *Nat. Chem. Biol. 5*, 217−219.

(12) Penkert, R. R., DiVittorio, H. M., and Prehoda, K. E. (2004) Internal recognition through PDZ domain plasticity in the Par-6-Pals1 complex. *Nat. Struct. Mol. Biol. 11*, 1122−1127.

(13) Hampson, L., Li, C., Oliver, A. W., Kitchener, H. C., and Hampson, I. N. (2004) The PDZ protein Tip-1 is a gain of function target of the HPV16 E6 oncoprotein. *Int. J. Oncol. 25*, 1249−1256.

(14) Kanamori, M., Sandy, P., Marzinotto, S., Benetti, R., Kai, C., Hayashizaki, Y., Schneider, C., and Suzuki, H. (2003) The PDZ protein tax-interacting protein-1 inhibits β-catenin transcriptional activity and growth of colorectal cancer cells. *J. Biol. Chem. 278*, 38758−38764.

(15) Reynaud, C., Fabre, S., and Jalinot, P. (2000) The PDZ protein TIP-1 interacts with the Rho effector rhotekin and is involved in Rho signaling to the serum response element. *J. Biol. Chem. 275*, 33962−33968.

(16) Banerjee, M., Huang, C., Marquez, J., and Mohanty, S. (2008) Probing the structure and function of human glutaminase-interacting protein: A possible target for drug design. *Biochemistry 47*, 9208−9219.

(17) Alewine, C., Olsen, O., Wade, J. B., and Welling, P. A. (2006) TIP-1 has PDZ scaffold antagonist activity. *Mol. Biol. Cell 17*, 4200−4211.

(18) Olalla, L., Gutierrez, A., Jimenez, A. J., Lopez-Tellez, J. F., Khan, Z. U., Perez, J., Alonso, F. J., de la Rosa, V., Campos-Sandoval, J. A., Segura, J. A., Aledo, J. C., and Marquez, J. (2008) Expression of the scaffolding PDZ protein glutaminase-interacting protein in mammalian brain. *J. Neurosci. Res. 86*, 281−292.

(19) Petrenko, V. A., Smith, G. P., Mazooji, M. M., and Quinn, T. (2002) α-Helically constrained phage display library. *Protein Eng. 15*, 943−950.

(20) Petrenko, V. A., Smith, G. P., Gong, X., and Quinn, T. (1996) A library of organic landscapes on filamentous phage. *Protein Eng. 9*, 797−801.

(21) Bax, A., and Davis, D. G. (1985) Mlev-17-Based Two-Dimensional Homonuclear Magnetization Transfer Spectroscopy. *J. Magn. Reson. 65*, 355−360.

(22) Bax, A., and Davis, D. G. (1985) Practical Aspects of Two-Dimensional Transverse NOE Spectroscopy. *J. Magn. Reson. 63*, 207−213.

(23) Otting, G., and Wüthrich, K. (1989) Extended heteronuclear editing of 2D ^{1}H NMR spectra of isotope-labeled proteins, using the X(ω1,ω2) double half filter. *J. Magn. Reson. 85*, 586−594.

(24) Zwahlen, C., Legault, P., Vincent, S. J. F., Greenblatt, J., Konrat, R., and Kay, L. E. (1997) Methods for Measurement of Intermolecular NOEs by Multinuclear NMR Spectroscopy: Application to a Bacteriophage λ N-Peptide/boxB RNA Complex. *J. Am. Chem. Soc. 119*, 6711−6721.

(25) Linge, J. P., Habeck, M., Rieping, W., and Nilges, M. (2003) ARIA: Automated NOE assignment and NMR structure calculation. *Bioinformatics 19*, 315−316.

(26) Yan, X., Zhou, H., Zhang, J., Shi, C., Xie, X., Wu, Y., Tian, C., Shen, Y., and Long, J. (2009) Molecular mechanism of inward rectifier potassium channel 2.3 regulation by tax-interacting protein-1. *J. Mol. Biol. 392*, 967−976.

(27) Zhang, J., Yan, X., Shi, C., Yang, X., Guo, Y., Tian, C., Long, J., and Shen, Y. (2008) Structural basis of β-catenin recognition by Tax-interacting protein-1. *J. Mol. Biol. 384*, 255−263.

(28) Zoetewey, D. L., Ovee, M., Banerjee, M., Bhaskaran, R., and Mohanty, S. (2011) Promiscuous binding at the crossroads of numerous cancer pathways: Insight from the binding of glutaminase interacting protein with glutaminase L. *Biochemistry 50*, 3528−3539.

(29) Bishop, T. C. (2009) VDNA: The virtual DNA plug-in for VMD. *Bioinformatics 25*, 3187−3188.

(30) Laskowski, R. A., Rullmannn, J. A., MacArthur, M. W., Kaptein, R., and Thornton, J. M. (1996) AQUA and PROCHECK-NMR: Programs for checking the quality of protein structures solved by NMR. *J. Biomol. NMR 8*, 477−486.

(31) Zencir, S., Ovee, M., Dobson, M. J., Banerjee, M., Topcu, Z., and Mohanty, S. (2011) Identification of brain-specific angiogenesis inhibitor 2 as an interaction partner of glutaminase interacting protein. *Biochem. Biophys. Res. Commun. 411*, 792−797.

(32) Kuzmicheva, G. A., Jayanna, P. K., Sorokulova, I. B., and Petrenko, V. A. (2009) Diversity and censoring of landscape phage libraries. *Protein Eng., Des. Sel. 22*, 9−18.

(33) Sidhu, S. S. (2005) in *Phage Display in Biotechnology and Drug Discovery* (Carmen, A., Ed.) Drug Discovery Series, Vol. 3, pp 1−748, CRC Press, Taylor & Francis Group, Boca Raton, FL.

(34) Katre, U. V., Mazumder, S., Prusti, R. K., and Mohanty, S. (2009) Ligand binding turns moth pheromone-binding protein into a pH sensor: Effect on the *Antheraea polyphemus* PBP1 conformation. *J. Biol. Chem. 284*, 32167−32177.

(35) Schultz, J., Hoffmuller, U., Krause, G., Ashurst, J., Macias, M. J., Schmieder, P., Schneider-Mergener, J., and Oschkinat, H. (1998) Specific interactions between the syntrophin PDZ domain and voltage-gated sodium channels. *Nat. Struct. Biol. 5*, 19−24.

(36) Wang, H., Yan, H., Fu, A., Han, M., Hallahan, D., and Han, Z. (2010) TIP-1 translocation onto the cell plasma membrane is a molecular biomarker of tumor response to ionizing radiation. *PLoS One 5*, e12051.

(37) Hariri, G., Yan, H., Wang, H., Han, Z., and Hallahan, D. E. (2010) Radiation-guided drug delivery to mouse models of lung cancer. *Clin. Cancer Res. 16*, 4968−4977.

(38) Sharma, S. C., Memic, A., Rupasinghe, C. N., Duc, A. C., and Spaller, M. R. (2009) T7 phage display as a method of peptide ligand discovery for PDZ domain proteins. *Biopolymers 92*, 183−193.

(39) Hillier, B. J., Christopherson, K. S., Prehoda, K. E., Bredt, D. S., and Lim, W. A. (1999) Unexpected modes of PDZ domain scaffolding revealed by structure of nNOS-syntrophin complex. *Science 284*, 812−815.

(40) Ludvigsen, M., Ostergaard, M., Vorum, H., Jacobsen, C., and Honore, B. (2009) Identification and characterization of endonuclein

binding proteins: Evidence of modulatory effects on signal transduction and chaperone activity. *BMC Biochem. 10*, 34.
(41) Ndong, J. d. L. C., Jean, D., Rousselet, N., and Frade, R. (2009) Down-regulation of the expression of RB18A/MED1, a cofactor of transcription, triggers strong tumorigenic phenotype of human melanoma cells. *Int. J. Cancer 124*, 2597−2606.
(42) Urbanik, T., Kohler, B. C., Boger, R. J., Worns, M. A., Heeger, S., Otto, G., Hovelmeyer, N., Galle, P. R., Schuchmann, M., Waisman, A., and Schulze-Bergkamen, H. (2011) Down-regulation of CYLD as a trigger for NF-κB activation and a mechanism of apoptotic resistance in hepatocellular carcinoma cells. *Int. J. Oncol. 38*, 121−131.
(43) Sun, S. C. (2010) CYLD: A tumor suppressor deubiquitinase regulating NF-κB activation and diverse biological processes. *Cell Death Differ. 17*, 25−34.
(44) Nishioka, M., Kohno, T., Tani, M., Yanaihara, N., Tomizawa, Y., Otsuka, A., Sasaki, S., Kobayashi, K., Niki, T., Maeshima, A., Sekido, Y., Minna, J. D., Sone, S., and Yokota, J. (2002) MYO18B, a candidate tumor suppressor gene at chromosome 22q12.1, deleted, mutated, and methylated in human lung cancer. *Proc. Natl. Acad. Sci. U.S.A. 99*, 12269−12274.
(45) Yanaihara, N., Nishioka, M., Kohno, T., Otsuka, A., Okamoto, A., Ochiai, K., Tanaka, T., and Yokota, J. (2004) Reduced expression of MYO18B, a candidate tumor-suppressor gene on chromosome arm 22q, in ovarian cancer. *Int. J. Cancer 112*, 150−154.